Available online at www.sciencedirect.com
SCIENCE DIRECT
Journal of Membrane Science 279 (2006) 301–310
journal of MEMBRANE SCIENCE
www.elsevier.com/locate/memsci

Modeling and experimental study of CO_2 absorption in a hollow fiber membrane contactor

Hong-Yan Zhang [a], Rong Wang [b,*], David Tee Liang [b], Joo Hwa Tay [a,b]

[a] *School of Civil and Environmental Engineering, Nanyang Technological University, Singapore 639798, Singapore*
[b] *Institute of Environmental Science & Engineering, Nanyang Technological University, Innovation Center (NTU), Block 2, Unit 237, 18 Nanyang Drive, Singapore 637723, Singapore*

Received 17 August 2005; received in revised form 29 November 2005; accepted 10 December 2005
Available online 19 January 2006

Abstract

In order to gain a better understanding of CO_2 absorption in a hollow fiber membrane contactor, theoretical simulations have been performed to describe CO_2 capture by distilled water and aqueous diethanolamine (DEA) solutions. The studies were focused on gas phase behaviors by taking the distributions of gas concentration and gas velocity along the flowing direction into account. The corresponding experiments were also carried out in a Celgard MiniModule to verify the simulated results.

In the case of physical absorption, both simulation and experimental results indicate that CO_2 flux increases with the liquid velocity, while the inlet gas velocity has no significant effect on CO_2 flux. The mass transfer resistance mainly exists on the liquid side. In the case of chemical absorption, the CO_2 flux is significantly influenced by the inlet gas velocity while the liquid velocity has a limited effect. The analyses of CO_2 concentration profiles in the gas and liquid phases as well as DEA concentration profile in the liquid phase reveal that CO_2 concentration in the gas phase serves as the rate-determining factor for the reaction between CO_2 and DEA. The significant CO_2 loss in the gas phase results in an interesting DEA concentration profile near the liquid–gas interface. There exists an effective module length L_{eff}, which suggests that increasing the module length is not a useful approach to enhance CO_2 absorption when the module length is longer than L_{eff}.

Keywords: Carbon dioxide capture; Chemical absorption; Amine solutions; Membrane contactors; Mass transfer; Numerical simulation

1. Introduction

Carbon dioxide (CO_2) has been considered to be a main contributor to the global warming. More than one-third of CO_2 emissions come from the combustion of fossil fuels in power plants worldwide [1]. Since we have to rely on fossil fuels to sustain economic growth besides achieving compliance with the Kyoto agreement, CO_2 capture from various gas streams, particularly from flue gas, has attracted extensive attentions. Among various techniques for CO_2 capture, the process of membrane contactor integrated with chemical absorption has become one of research focuses for decades because of its advantages over the traditional gas absorption processes, such as independent liquid and gas flow rate manipulation, much larger gas–liquid interfaces and the flexibility to scale up or down [2–16].

In order to understand the process of CO_2 capture in the membrane contactor, many theoretical and experimental studies have been conducted to investigate the effects of various factors on the separation efficiency of the system. Usually, physical absorption was studied as a starting point. In the work of Kreulen et al. [8], a mass transfer model based on the diffusion theory was developed for the liquid phase, and Graetz–Leveque equation was employed by assuming that the mass transfer in a hollow fiber is analogous to the heat transfer in a laminar flow through a circular duct. The effects of the fiber diameter, liquid viscosity and liquid velocity on the mass transfer were evaluated. Recently, Dindore et al. [17] developed a physical absorption model for cross flow modules by describing the gas flow with a mixing-cell model and the liquid flow with diffusion differential equations. They found that even for the physical absorption, the CO_2 concentration distribution in the gas phase has a considerable influence on the CO_2 flux in the case of high CO_2 removal.

Chemical absorption, which can find many practical applications, was also widely studied by different research groups.

* Corresponding author. Tel.: +65 6794 3764; fax: +65 6792 1291.
E-mail address: rwang@ntu.edu.sg (R. Wang).

0376-7388/$ – see front matter © 2005 Elsevier B.V. All rights reserved.
doi:10.1016/j.memsci.2005.12.017

Kreulen et al. [9] established a model to describe CO_2 absorption by a hydroxide solution. By assuming constant gas concentration, they simulated the local CO_2 flux and local enhancement effect as a function of the fiber length. However, as for the effect of liquid or gas velocity on the CO_2 flux, no theoretical results were given to compare with the experimental data. Lee et al. [18], Kumar et al. [19], Yeon et al. [20] and Wang et al. [21] also built up similar models for CO_2 removal by amine solutions or hydroxide solutions with the assumption of constant CO_2 concentration in the gas phase or using pure CO_2. Since the CO_2 concentration in the gas phase was assumed to remain unchanged in the contactor, the effect of gas phase on the CO_2 absorption was not well understood. Efforts to understand the effects of gas behavior on the mass transfer are on going. Different from above cases, Karoor et al. developed a differential model for both liquid and gas phases. However, the mass transfer could not be well predicted by the model for the system of CO_2/N_2 mixture [7,22]. Hoff et al. [23] assumed the gas phase as a plug flow in the simulation. Probably because of low CO_2 concentration in the gas phase, the gas flow rate was not found to have an obvious effect on the mass transfer coefficient, which is different from the results presented by Kreulen et al. [9]. In summary, despite many efforts taken to develop various models, the gas phase behavior in the chemical absorption has not been given much attention in the most of process simulations.

In this paper, a numerical simulation was performed to describe both physical and chemical absorptions of CO_2 from CO_2/N_2 mixture using distilled water and a 2 M aqueous diethanolamine (DEA) solution as the absorbent, respectively. The study was focused on the gas phase behavior where the distributions of gas concentration and gas velocity along the flow direction were taken into account in the modeling. The corresponding experiments were also carried out in a Celgard MiniModule to verify simulated results.

2. Theory

2.1. Reaction mechanism

Zwitterion mechanism has been commonly accepted as the reaction mechanism between CO_2 and primary or secondary amines. Originally proposed by Caplow [24] and reintroduced by Danckwerts [25], the mechanism can be represented as two steps as follows [24,25]:

$$CO_2 + R_1R_2NH \underset{k_{-1}}{\overset{k_2}{\rightleftharpoons}} R_1R_2NH^+COO^- \quad (1)$$

$$R_1R_2NH^+COO^- + B \xrightarrow{k_b} R_1R_2NCOO^- + BH^+ \quad (2)$$

In the first step, CO_2 reacts with DEA to form zwitterions, which are deprotonated by the bases denoted as B in the solution in the second step. In the aqueous DEA solution, the bases are DEA, water and hydroxyl ion [26].

Based on the assumption of quasi-steady-state condition for the zwitterions concentration, the rate of CO_2 reaction with DEA was derived as [27–31]:

$$r_A = \frac{[DEA][CO_2]}{\frac{1}{k_2} + \frac{1}{(k_2 k_{H_2O}/k_{-1})[H_2O] + (k_2 k_{OH^{-1}}/k_{-1})[OH^{-1}] + (k_2 k_{DEA}/k_{-1})[DEA]}} \quad (3)$$

where the effect of hydroxyl ion (OH^{-1}) can be neglected without causing a substantial loss of accuracy [27] and the kinetic parameters are listed in Table 1.

Table 1
Kinetic parameters of reaction between CO_2 and DEA at 298 K

DEA concentration (mol m^{-3})	150–2500
k_2 (m^3 mol^{-1} s^{-1})	2.375
$\frac{k_2 k_{H_2O}}{k_{-1}}$ (m^6 mol^{-2} s^{-1})	2.20E-06
$\frac{k_2 k_{DEA}}{k_{-1}}$ (m^6 mol^{-2} s^{-1})	4.37E-04
Reference	[31]

2.2. Model development

A numerical model was developed to describe CO_2 capture from the mixture of CO_2/N_2 by distilled water or an aqueous DEA solution. As shown in Fig. 1, there are three mass transfer regions for CO_2 absorption in a membrane contactor: mass transfer in the liquid phase, mass transfer in the gas phase and mass transfer through the membrane. The liquid absorbent was assumed to flow in the lumen of the membrane while the gas mixture of CO_2/N_2 with 20/80 volume ratio flows in the shell side co-currently. Since the fiber length is not very long, the co-current flow arrangement can simplify the calculation tremendously. Following assumptions have been adopted: (1) a steady state and isothermal condition have been achieved; (2) the axial diffusion is negligible; (3) a fully developed parabolic liquid velocity profile is presented within the lumen of the hollow fiber; (4) ideal gas behavior is valid for gas phase; (5) Henry's law is applicable.

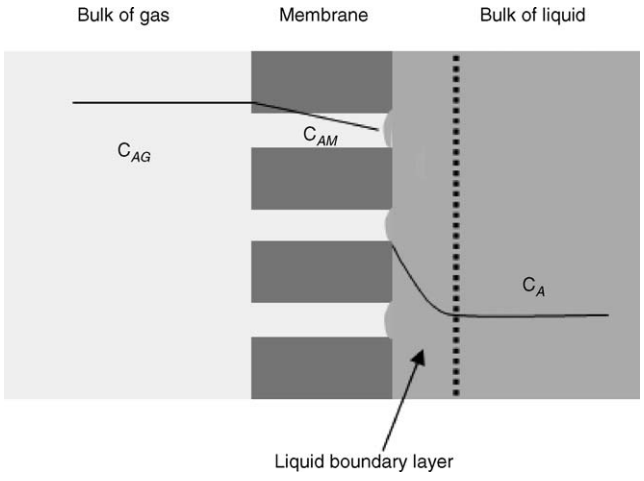

Fig. 1. Mass transfer regions in hydrophobic membrane contactors for CO_2 absorption.

Table 2
Physical properties of CO_2 in water and 2 M aqueous DEA solution

Absorbent	Component	Solubility (mol/mol)	Diffusivity (m^2/s)	Viscosity (Pa s)
Water	CO_2	0.833	1.92E-9	8.90E-4
2 M aqueous DEA solution	CO_2	0.765	1.047E-9	1.90E-3
	DEA	–	4.967E-10	

2.2.1. Mass transfer in the liquid phase

Based on above assumptions, the conservation equation for the mass transfer in the liquid phase can be derived as

$$v_z \frac{\partial C_A}{\partial z} = D_A \frac{\partial^2 C_A}{\partial r^2} + \frac{D_A}{r}\frac{\partial C_A}{\partial r} - r_A \quad (4)$$

$$v_z \frac{\partial C_B}{\partial z} = D_B \frac{\partial^2 C_B}{\partial r^2} + \frac{D_B}{r}\frac{\partial C_B}{\partial r} - r_B \quad (5)$$

where the subscripts of A and B denote CO_2 and DEA, respectively. The liquid axial velocity profile is given as

$$v_z = 2U_L\left[1 - \left(\frac{r}{R}\right)^2\right] \quad (6)$$

The initial and boundary conditions are

$$z = 0, \quad C_A = 0, \quad C_B = C_{B0} \quad (7)$$

$$r = 0, \quad \frac{\partial C_A}{\partial r} = 0, \quad \frac{\partial C_B}{\partial r} = 0 \quad (8)$$

$$r = R_i, \quad C_A = HC_{AM,R_i}, \quad \frac{\partial C_B}{\partial r} = 0 \quad (9)$$

where a symmetry in the radial direction of hollow fibers and non-volatile DEA are assumed. The Henry's law is applied to connect CO_2 interfacial concentrations in the liquid and membrane phase. The physical properties (solubility and diffusivity) of CO_2 in water and 2 M aqueous DEA solutions are listed in Table 2, which were cited or calculated with the methods introduced in the reference [32].

2.2.2. Mass transfer in the gas phase

The gas flow in the shell side of the membrane contactor can be configured as fluid envelope around the fiber (Fig. 2) and there is no interaction between fibers. The dimension of the free surface can be estimated by Happel's free surface model [33]:

$$R_e = \left(\frac{1}{1-\varepsilon'}\right)^{1/2} R_0 \quad (10)$$

Considering that the CO_2 diffusivity in gas phase is much higher than that in liquid phase [34], it is reasonable to assume the gas flow as plug flow, which implies that the gas velocity and concentration distributions in the radial direction can be ignored in the shell side. For a segment with a length of Δz in the axial direction (Fig. 3), the mass balance can be written as

$$\Delta n_{AG} = C_{AG}\Delta U_G A_G + \Delta C_{AG} U_G A_G + \Delta C_{AG}\Delta U_G A_G \quad (11)$$

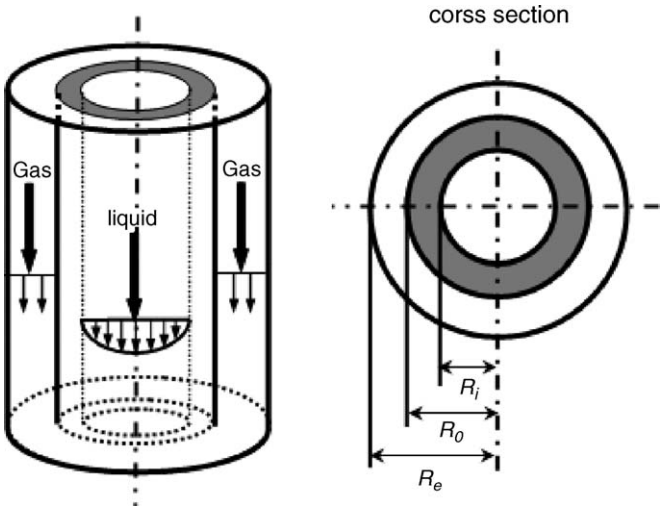

Fig. 2. Schematic diagram of the liquid and gas flow in a hollow fiber.

Under the operation pressure (normal pressure), the ideal gas law is applied to the gas phase:

$$\frac{P}{RT}\Delta U_G A_G = \Delta n_{AG} \quad (12)$$

Combining Eqs. (11) and (12), the CO_2 removal rate in the segment can be derived as

$$\Delta n_{AG} = \frac{\Delta C_{AG} U_G A_G}{1 - \frac{RT}{P}\Delta C_{AG} - \frac{RT}{P} C_{AG}} \quad (13)$$

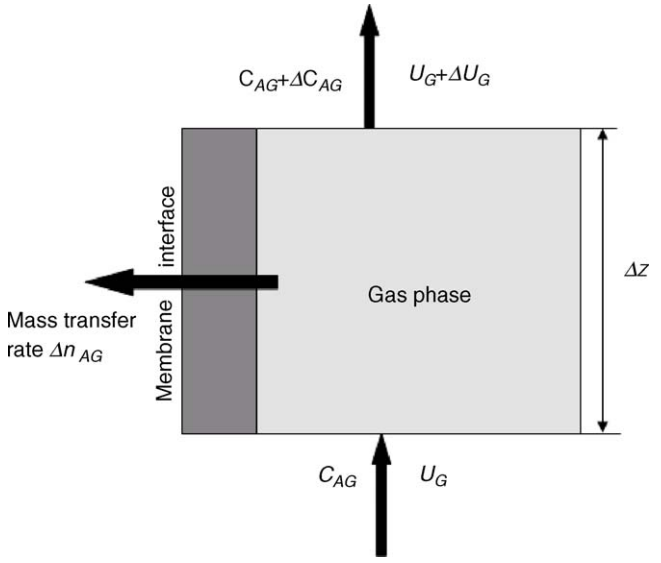

Fig. 3. Schematic diagram of mass transfer in gas phase.

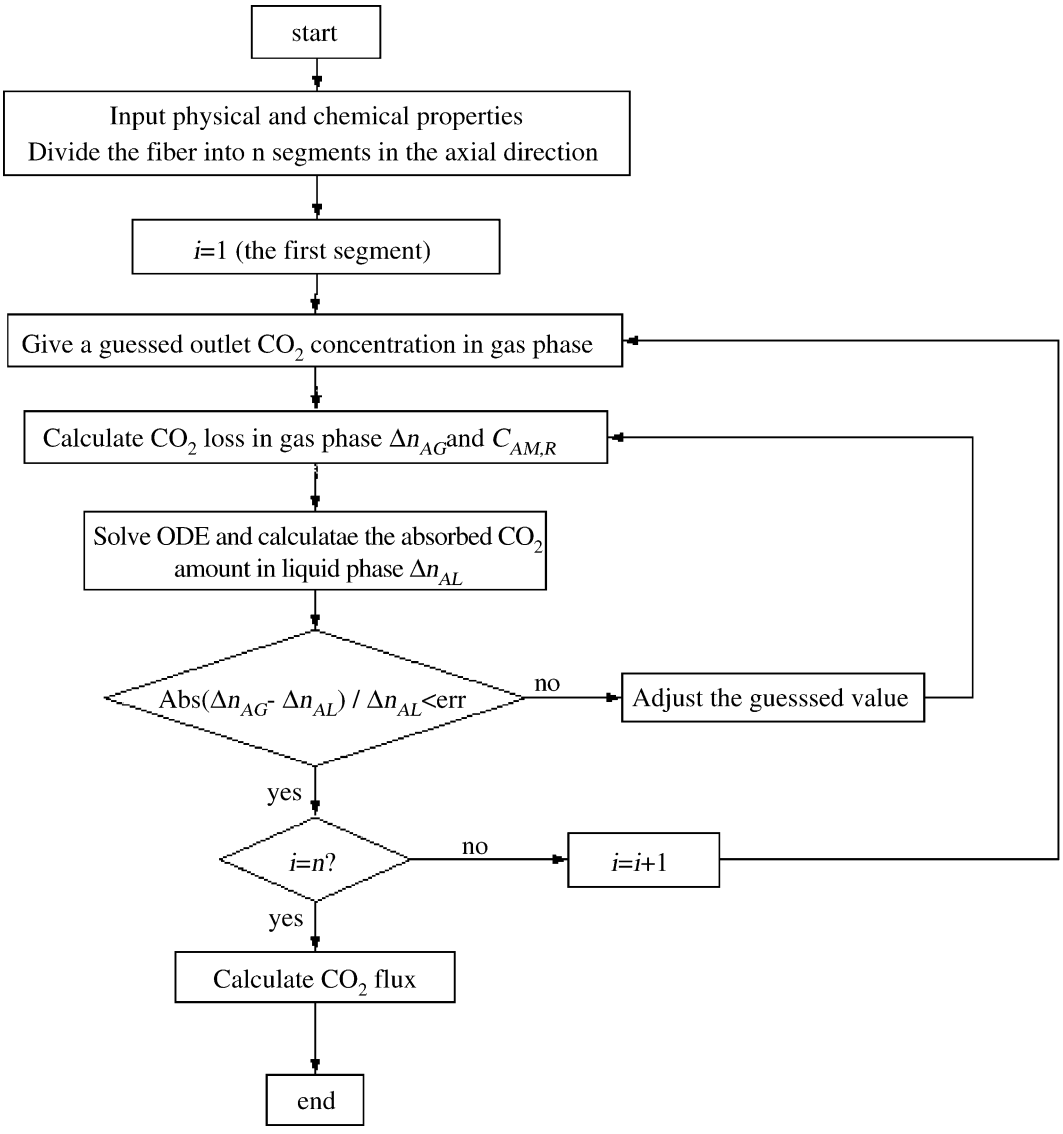

Fig. 4. Computation flow chart.

2.2.3. Mass transfer in the membrane phase

In the membrane phase, the mass transfer rate in a segment with a length of Δz can be expressed by

$$\Delta n_{\mathrm{AM}} = \frac{\varepsilon D_{\mathrm{G}}}{\tau} \frac{C_{\mathrm{AG,av}} - C_{\mathrm{AM},R_i}}{R_0 - R} 2\pi R\, \Delta z \tag{14}$$

where Δn_{AM} is equal to Δn_{AG} based on mass conservation.

2.3. Numerical scheme

Along the axial direction, the fiber was divided into many small segments with an equivalent length of Δz. In each segment, a set of partial differential equations (Eqs. (4)–(9)) was used to describe the mass transfer in liquid phase while Eqs. (13) and (14) were employed to describe the mass transfer in the gas phase and membrane phase, respectively. In order to reduce the partial differential equations to ordinary differential equations, a method of line (MOL) [7,9,35] was applied and the discretization was carried out in the radial direction.

By giving a guessed value of the gas phase CO_2 concentration at the outlet of the first segment, Δn_{AG} and $C_{\mathrm{AM},R}$ were calculated via Eqs. (13) and (14). Then the ordinary differential equations can be solved with their initial and boundary conditions which contained $C_{\mathrm{AM},R}$ using MATLAB. After obtaining the concentration profiles of CO_2 and DEA at the inlet and outlet of the segment, the CO_2 mass transfer rate Δn_{AL} in the liquid phase can be calculated by integrating the CO_2 concentration along the radial direction. Since CO_2 loss in the gas phase (Δn_{AG}) should be equal to the gain in the liquid phase (Δn_{AL}), the initially guessed value of the gas phase CO_2 concentration at the outlet of the first segment was adjusted until the difference between Δn_{AG} and Δn_{AL} was acceptable. Similar procedures were taken to calculate the following segments. The algorithm is given schematically in Fig. 4.

Table 3
Specifications of the membrane contactor used

Module length (mm)	188
Fiber o.d. (μm)	300
Fiber i.d. (μm)	220
Fiber length (mm)	113
Number of fibers	1100
Pore size (μm)	0.04
Porosity	0.40
Contact area (m^2)	0.09

3. Experimental

A Celgard microporous hollow fiber MiniModule® 0.75 × 5, which was kindly provided by Celgard Inc., was used as a contactor in this study. The hollow fibers in the module were X-50 type and made of polypropylene. The characteristics of the membrane contactor are listed in Table 3. A 99.5% grade DEA purchased from Merck was dissolved in distilled water to prepare aqueous 2 M solutions.

The experimental setup is schematically presented in Fig. 5. CO_2/N_2 mixture with a volume ratio of 20/80 was used as the feed gas while the N_2 saturated distilled water or aqueous 2 M DEA solution was used as the absorbent. In this study, the gas always passed through the shell side and the liquid flowed cocurrently through the lumen side of the hollow fibers.

In a typical experiment, the feed gases were introduced into the system from compressed gas cylinders and the flow rates were adjusted by mass flow controllers (Brooks Instrument MFC 5850). The gas pressures were indicated by the pressure gauges at the shell inlet and outlet. The gas volume flow rates at the inlet and the outlet were measured by a digital bubble meter. The compositions of the inlet and the outlet gas streams were analyzed using a Varian Micro GC continuously.

A digital variable flow gear pump (Tuthill) was used to control the liquid flow and pumped the liquid into the lumen side of hollow fibers from a 10 l container. The pressures at the inlet and the outlet of the lumen side were recorded. The liquid flow rate was also checked at the outlet at regular intervals. The CO_2 concentration of the outlet liquid was measured by a CO_2 electrode (Thermo Orion model 95-02) to verify the mass balance via the gas analysis. The measurement range of the electrode was 4.4–440 ppm CO_2 with a maximum error of ±2%.

For each run of experiment, the system was operated for at least half an hour to ensure that a steady state has been achieved before any data collection. All the experiments were conducted at the room temperature of 25 °C.

4. Results and discussion

4.1. CO_2 absorption with water

The physical absorption of CO_2 from CO_2/N_2 (20/80 in volume ratio) mixture was simulated by neglecting the reaction rates: r_A and r_B in Eqs. (4) and (5). As shown in Fig. 6, the calculated CO_2 flux (J_{CO_2}) increases with the liquid velocity (U_L), which is in good agreement with experimental data (the deviation is less than 8%). In contrast, the inlet gas velocity has no significant effect on J_{CO_2}. It implies that in the case of physical absorption, the mass transfer resistance mainly exists on the liquid side. To further understand it, the CO_2 concentration profiles in the liquid phase at three different liquid velocities are presented in Fig. 7. From this figure it can be seen that the higher the liquid velocity, the lower the CO_2

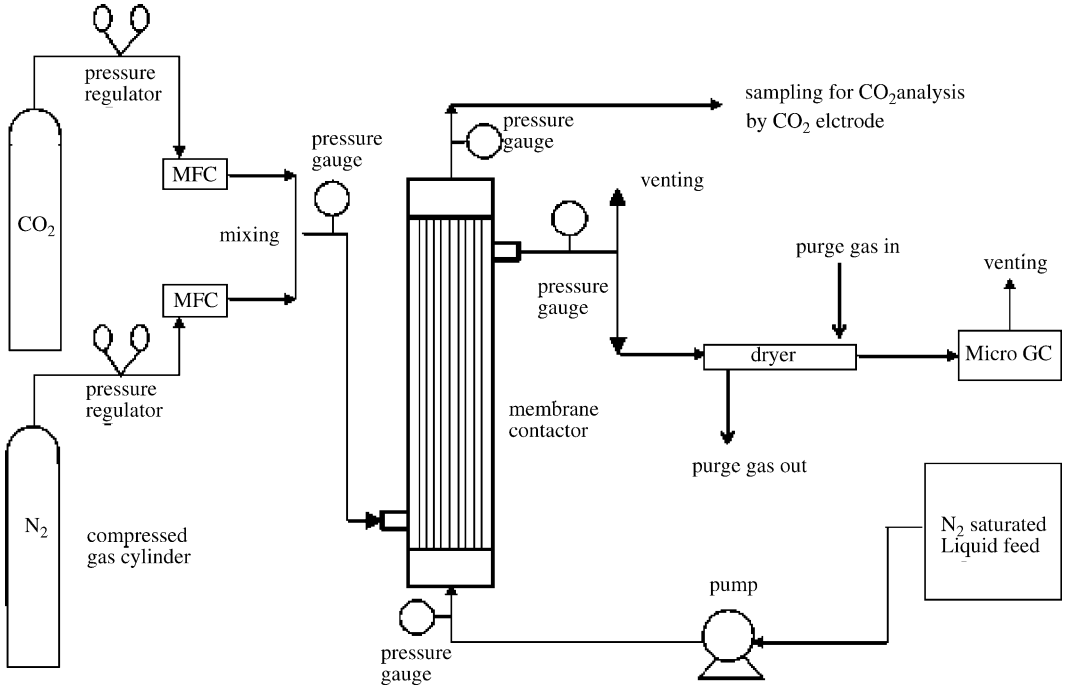

Fig. 5. Experimental setup of CO_2 absorption in a membrane contactor.

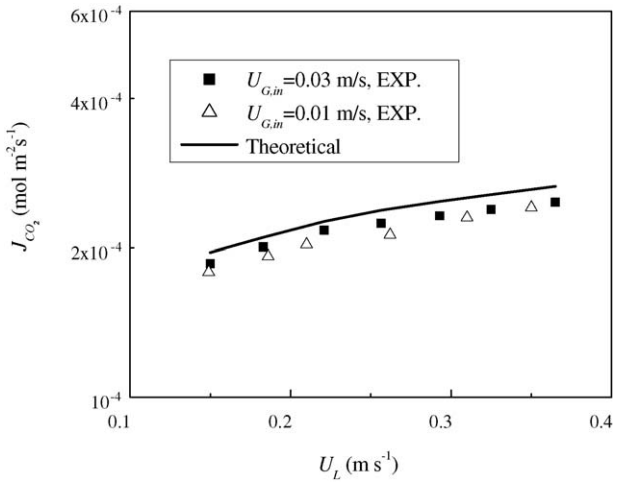

Fig. 6. Effect of the liquid velocity on CO_2 flux at different inlet gas velocities (feed gas: 20/80 CO_2/N_2 mixture; absorbent: distilled water).

concentration profile is. This is because when distilled water is supplied at a higher speed, the consumed distilled water is replaced by more fresh water, resulting in a lower average CO_2 concentration in the liquid phase. Thus, the driving force for CO_2 transfer is increased, leading to a higher CO_2 flux.

4.2. CO_2 absorption with 2 M aqueous DEA solutions

In the case of 2 M aqueous DEA solutions being used as the absorbent, the CO_2 absorption from the CO_2/N_2 mixture is enhanced by the chemical reaction. Figs. 8 and 9 show the axial gas CO_2 concentration and gas velocity distributions for both chemical and physical absorptions, respectively. It can be seen that at the same operating conditions, the gas CO_2 concentration and gas velocity in the chemical absorption drop about 90% and 20% each throughout the fiber, which are much higher than 20% and 5% of the counterparts in the physical absorption. It demonstrates that chemical absorption is more effective to remove CO_2.

The effect of liquid velocity on CO_2 flux is presented in Fig. 10. As shown in this figure, experimental data match the simulation results quite well. It was also noticed that the CO_2 flux (J_{CO_2}) changes with the liquid velocity (U_L) in a way dif-

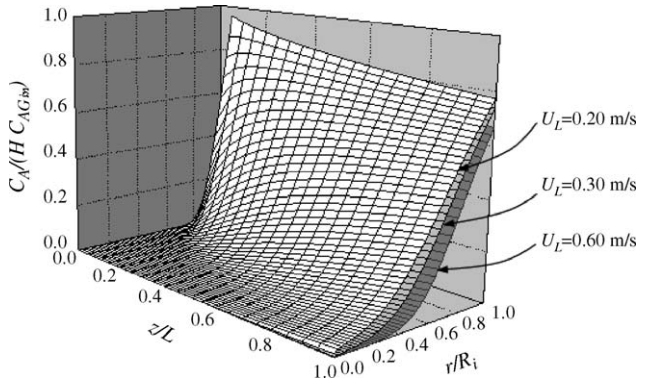

Fig. 7. CO_2 concentration profile in the liquid phase at liquid velocities of 0.20, 0.30 and 0.60 m/s (feed gas: 20/80 CO_2/N_2 mixture; absorbent: distilled water).

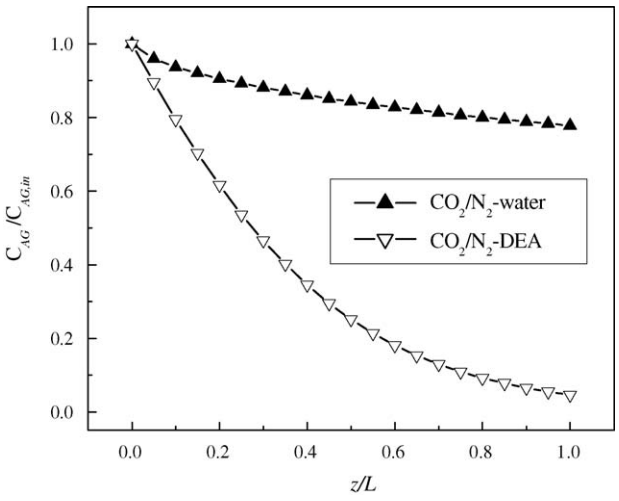

Fig. 8. CO_2 concentration distribution along the fiber in the gas phase (feed gas: 20/80 CO_2/N_2 mixture; absorbent: 2 M aqueous DEA and distilled water, U_L = 0.15 m/s, $U_{G,in}$ = 0.073 m/s).

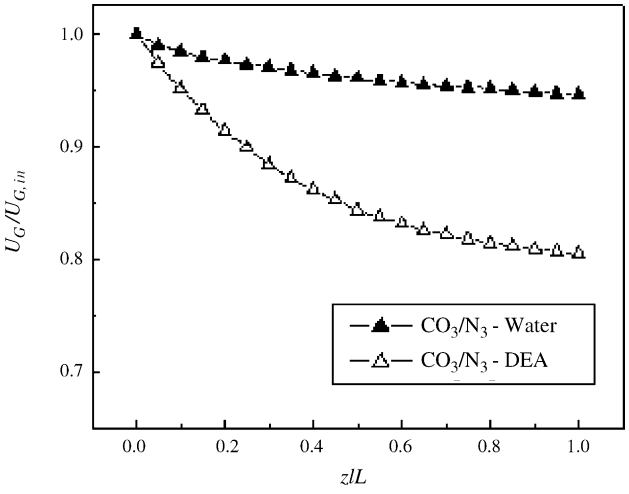

Fig. 9. Gas velocity distribution along the fiber (feed gas: 20/80 CO_2/N_2 mixture; absorbent: 2 M aqueous DEA and distilled water, U_L = 0.15 m/s, $U_{G,in}$ = 0.073 m/s).

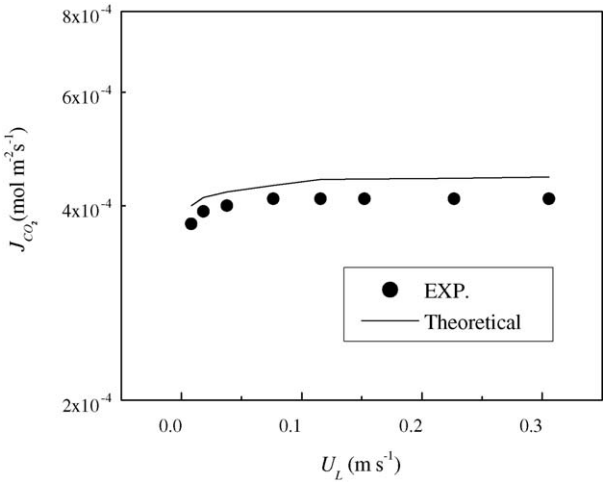

Fig. 10. Effect of the liquid velocity on CO_2 flux at inlet gas velocity of 0.041 m/s (feed gas: 20/80 CO_2/N_2 mixture; absorbent: 2 M aqueous DEA solution).

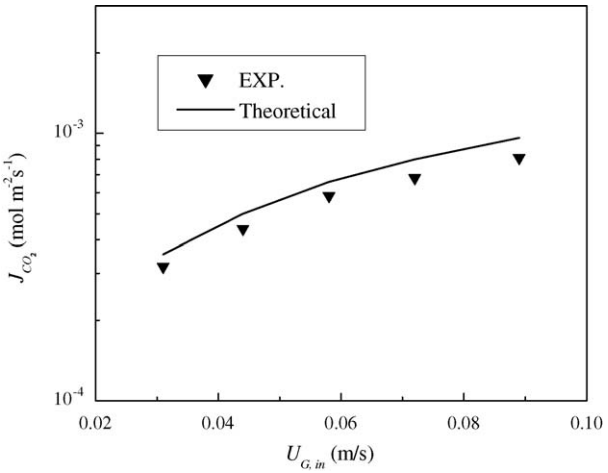

Fig. 11. Effect of the gas velocity on CO_2 flux at liquid velocity of 0.15 m/s (feed gas: 20/80 CO_2/N_2 mixture; absorbent: 2 M aqueous DEA solution).

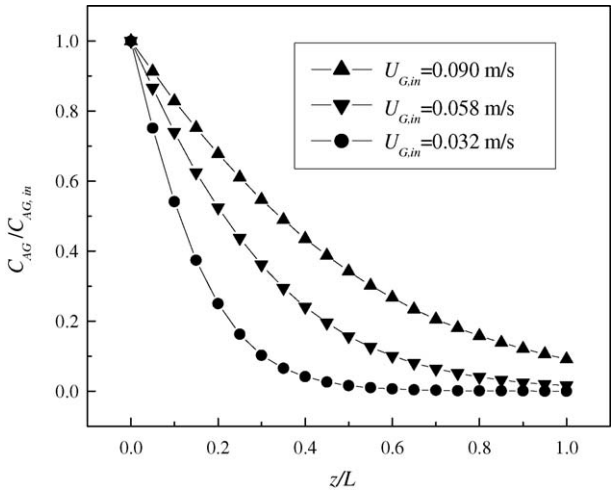

Fig. 12. Gas phase CO_2 concentration distribution in the axial direction at different inlet gas velocities (feed gas: 20/80 CO_2/N_2 mixture; absorbent: 2 M aqueous DEA, U_L = 0.15 m/s).

ferent from that of physical absorption. In the regime of very low liquid velocity ($U_L < 0.05$ m/s), the CO_2 absorption flux increases with the liquid velocity. This is probably due to the significant depletion of active amines in the solution. With a further increase of the liquid velocity, the supply of the active amines is accelerated and the depletion could be mitigated effectively. Thus in the regime where the liquid velocity is relatively high ($U_L > 0.1$ m/s), the CO_2 flux is almost not affected by the liquid velocity. From the viewpoint of applications, the high velocity regime is ideally suitable for the operation of membrane contactors and therefore, our subsequent studies were focused on this regime.

The impact of inlet gas velocity ($U_{G,in}$) on the CO_2 flux (J_{CO_2}) is depicted in Fig. 11. Modeling results predict that the increase of gas velocity could effectively enhance the CO_2 mass transfer, which is confirmed by experiments. To gain an insight into this observation, the CO_2 concentration profiles in the gas and liquid phases as well as DEA concentration profiles were examined, as the CO_2 mass transfer is influenced not only by the gas phase CO_2 concentration but also by the liquid phase DEA concentration [9,14,20].

Fig. 12 shows gas phase CO_2 concentration profiles in the axial direction at different inlet gas velocities. It can be seen that CO_2 concentration decreases considerably from the inlet to the outlet of the membrane module. However, when more CO_2 is introduced into the module, the depletion of CO_2 is slowed down. As a result, the higher the inlet gas velocity, the greater the average CO_2 concentration in the gas phase throughout the module. As for the CO_2 concentration in the liquid phase, there is a steep drop near the liquid–gas interface at the membrane wall ($r/R \rightarrow 1$) while it is almost zero in the rest of the liquid phase, as illustrated in Fig. 13. It indicates that most of amine solutions are still intact in the liquid phase, which is confirmed by the DEA concentration profile shown in Fig. 14. Although the DEA concentration drops significantly near the membrane wall in the inlet regime, the overall depletion rate of DEA is much smaller than that of CO_2 in the gas phase as shown in Fig. 12. As such, the DEA concentration can be considered almost unchanged except

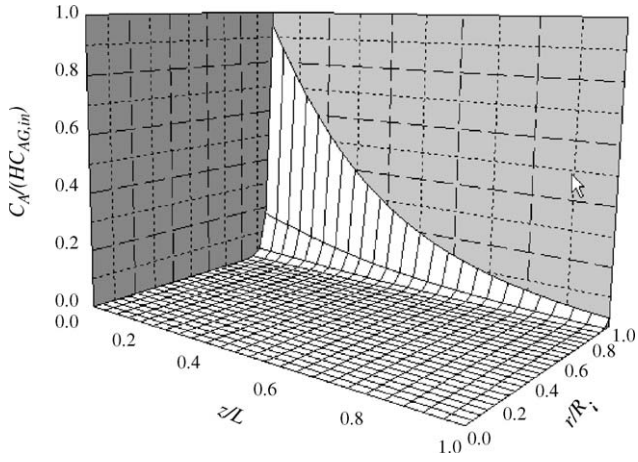

Fig. 13. Liquid phase CO_2 concentration profile in radial direction (feed gas: 20/80 CO_2/N_2 mixture; absorbent: 2 M aqueous DEA, U_L = 0.15 m/s, $U_{G,in}$ = 0.073 m/s).

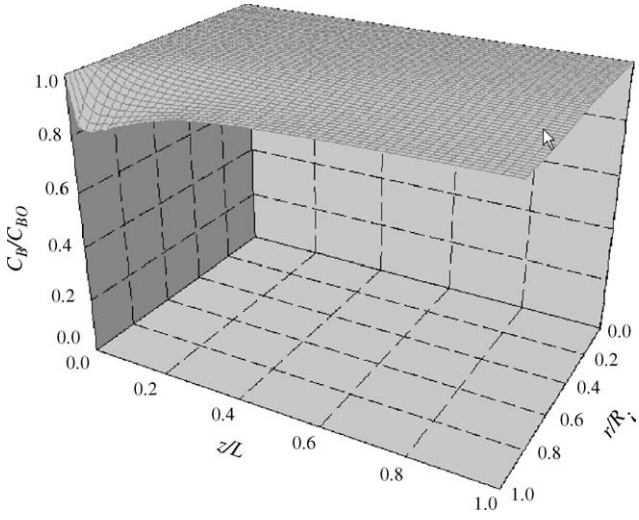

Fig. 14. Liquid phase DEA concentration profile in the lumen of a hollow fiber (feed gas: 20/80 CO_2/N_2 mixture; absorbent: 2 M aqueous DEA, U_L = 0.15 m/s, $U_{G,in}$ = 0.073 m/s).

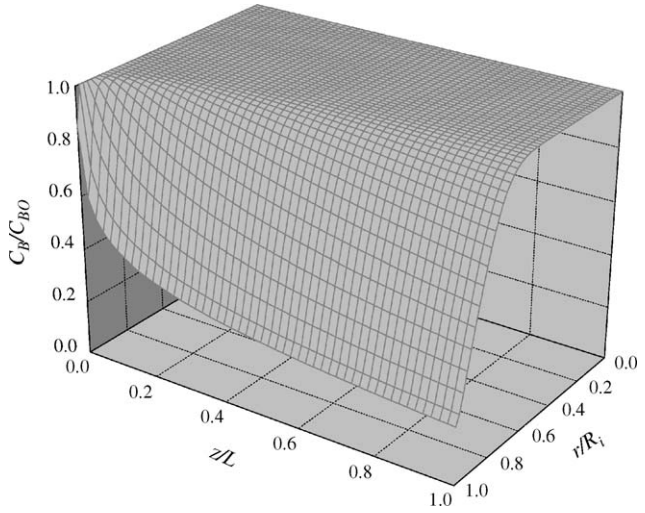

Fig. 15. Liquid phase DEA concentration profile with constant CO_2 concentration in gas phase (feed gas: 20/80 CO_2/N_2 mixture; absorbent: 2 M aqueous DEA, $U_L = 0.15$ m/s, $U_{G,in} = 0.073$ m/s).

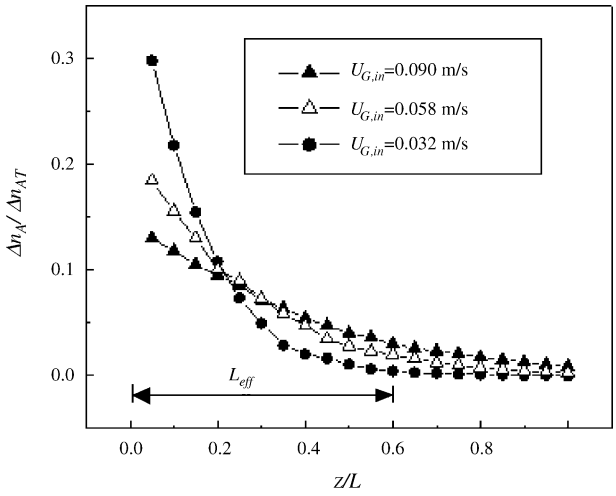

Fig. 16. The percentage of absorbed CO_2 over total absorbed CO_2 at different axial positions (feed gas: 20/80 CO_2/N_2 mixture; absorbent: 2 M aqueous DEA, $U_L = 0.15$ m/s).

in the area adjacent to the liquid–gas interface in the inlet regime. It implies that DEA has sufficient capacity to absorb CO_2. Therefore, it is reasonable to assume that the reaction between CO_2 and DEA is pseudo first order and the CO_2 concentration in the gas phase serves as the rate-determining factor. This also explains why the effect of increasing liquid velocity on CO_2 flux is limited. Similar conclusion was also drawn in literature [9]. Since a higher inlet gas velocity makes a higher average CO_2 concentration in the gas phase, a higher CO_2 flux is thus anticipated.

From Fig. 14, it was also noticed that there exists a concentration valley near the membrane wall in the inlet regime, where the DEA concentration decreases tremendously then increases along the rest of the module. In contrast, in the area far away from the liquid–gas interface, the DEA concentration only slightly decreases along the axial position. This is believed to be caused by the strong chemical reaction between DEA and CO_2 in the near-wall inlet regime, where both DEA and CO_2 have highest initial concentrations. Due to the significant CO_2 loss in the gas phase, the reaction rate tends to decrease greatly in the following area which in turn resulted in much less consumption of DEA. Meanwhile, in the radial direction, the DEA diffusion towards the interface also facilitates the recovery of DEA loss. Consequently, the DEA concentration shows a trend of gradual increase after initial decrease in the first several segments.

To confirm that such a DEA concentration profile is mainly resulted from significant CO_2 loss in the gas phase, a comparative simulation test was performed where the CO_2 concentration change in the gas phase is ignored. As presented in Fig. 15, the DEA concentration decreases monotonically along the axial direction in the area adjacent to the liquid–gas interface where a constant CO_2 concentration is assumed throughout the fiber.

According to Fig. 12, the CO_2 concentration decreases gradually along the membrane module. Thus, the fiber was divided equally into 20 segments to calculate the percentage of the absorbed CO_2 in each segment over the total absorbed amount at different inlet gas velocities. From Fig. 16, it was interesting to find out that the CO_2 absorption is mainly conducted in the front segments near the inlet. For example, when $U_{G,in}$ is 0.032 m/s, CO_2 is mainly absorbed in the segments up till $z/L = 0.6$ while the CO_2 absorption is negligible in the rest segments. Therefore, there exists an effective length L_{eff} to reflect this observation. Nevertheless, the effective length varies with the gas inlet velocity as shown in Fig. 16. Although increasing the gas velocity can increase the effective length, approximately 20% of the total segments have little absorption capacity under current conditions. This reminds us that increasing the length of the membrane module is not an effective approach to enhance CO_2 absorption when the membrane module is longer than L_{eff}.

5. Conclusion

Theoretical modeling and experiments have been performed to study the physical and chemical absorptions of CO_2 using distilled water and 2 M aqueous DEA solutions as the absorbent, respectively. All the experiments were carried out in a Celgard MiniModule membrane contactor.

In the case of physical absorption, both simulation and experimental results indicate that CO_2 flux increased with the liquid velocity, while the inlet gas velocity has no significant influence on CO_2 flux. The mass transfer resistance mainly exists on the liquid side.

The CO_2 absorption has been enhanced greatly in a 2 M DEA aqueous solution. The CO_2 flux is influenced significantly by the gas velocity while the liquid velocity has a limited effect on the CO_2 transfer. The analyses of the CO_2 concentration profiles in the gas and liquid phases as well as the DEA concentration profile indicate that the CO_2 concentration in the gas phase serves as the rate-determining factor for the reaction between CO_2 and DEA. The significant drop of CO_2 concentration in the inlet regime also results in an interesting DEA concentration profile near the liquid–gas interface. There exists an effective module length L_{eff}, which suggests that increasing the module length

is not a useful approach to enhance CO_2 absorption when the module length is longer than L_{eff}.

Acknowledgements

The authors gratefully acknowledge the support of Agency of Science, Technology and Research of Singapore (A*STAR) for funding this research with the grant number of 032 101 0024.

Nomenclature

A_G	cross sectional area for gas flow in a mass transfer segment (m^2)
C_A	concentration of carbon dioxide in liquid phase ($mol\,m^{-3}$)
C_{AG}	concentration of carbon dioxide in gas phase ($mol\,m^{-3}$)
C_{AM}	concentration of carbon dioxide in membrane phase ($mol\,m^{-3}$)
C_{AM,R_i}	concentration of carbon dioxide at R_i position in membrane phase ($mol\,m^{-3}$)
C_B	concentration of DEA in liquid phase ($mol\,m^{-3}$)
C_{B0}	concentration of DEA in liquid phase at inlet ($mol\,m^{-3}$)
D_A, D_B	diffusion coefficients of carbon dioxide and DEA in liquid phase, respectively ($m^2\,s^{-1}$)
D_G	diffusion coefficient of carbon dioxide in gas phase ($m^2\,s^{-1}$)
H	Henry's constant ($H = [CO_2]_{\surd}/[CO_2]_g$ at equilibrium)
J_{CO_2}	absorption flux of carbon dioxide ($mol\,m^{-3}\,s^{-1}$)
L	length of hollow fibers (m)
L_{eff}	effective mass transfer length of hollow fibers (m)
Δn_A	carbon dioxide mass transfer rate in a segment ($mol\,s^{-1}$)
Δn_{AT}	total carbon dioxide mass transfer rate in all the segments ($mol\,s^{-1}$)
P	operation pressure in gas phase (kPa)
r	radial coordinate (m)
r_A	rate of carbon dioxide reaction in liquid phase ($mol\,m^{-3}\,s^{-1}$)
r_B	rate of DEA reaction in liquid phase ($mol\,m^{-3}\,s^{-1}$)
R	gas constant ($8.314\,J\,mol^{-1}\,K^{-1}$)
R_e	external radius of a hollow fiber (m)
R_i	internal radius of a hollow fiber (m)
R_0	radius of gas free surface (m)
T	operation temperature (K)
U_L	average liquid velocity ($m\,s^{-1}$)
$U_{G,in}$	gas velocity at the inlet ($m\,s^{-1}$)
v_z	liquid velocity in axial direction at radial position of r ($m\,s^{-1}$)
z	axial coordinate (m)
Δz	length of a mass transfer segment (m)

Greek letters

ε	membrane porosity
ε'	shell-side void volume fraction of a hollow fiber module
τ	tortuosity of membrane pores

Subscripts

A	carbon dioxide
av	average
B	diethanolamine
G	gas phase
in	inlet
L	liquid phase
M	membrane phase

References

[1] IEA Greenhouse Gas R&D Programme, Putting carbon back into the ground. Online Report, 2001, available at: http://www.ieagreen.org.uk/ccs.html.
[2] A. Gabelman, S.T. Hwang, Hollow fiber membrane contactors, J. Membr. Sci. 159 (1999) 61–106.
[3] Q. Zhang, E.L. Clussler, Microporous hollow fibers for gas absorption. I. Mass transfer in the liquid, J. Membr. Sci. 23 (1985) 321–332.
[4] Q. Zhang, E.L. Cussler, Microporous hollow fibers for gas absorption. II. Mass transfer across the membrane, J. Membr. Sci. 23 (1985) 333–345.
[5] M.C. Yang, E.L. Cussler, Designing hollow-fiber contactors, AIChE J. 32 (1986) 1910–1916.
[6] E.L. Cussler, in: G. Joao, et al. (Eds.), Hollow Fiber Contactors in Membrane Processes in Separation and Purification, Kluwer Academic Publishers, 1994.
[7] S. Karoor, K.K. Sirkar, Gas absorption studies in microporous hollow fiber membrane modules, Ind. Eng. Chem. Res. 32 (1993) 674–684.
[8] H. Kreulen, C.A. Smolders, G.F. Versteeg, W.P.M. van Swaaij, Microporous hollow fibre membrane modules as gas–liquid contactors. Part 1. Physical mass transfer processes: a specific application: mass transfer in highly viscous liquids, J. Membr. Sci. 78 (1993) 197–216.
[9] H. Kreulen, C.A. Smolders, G.F. Versteeg, W.P.M. van Swaaij, Microporous hollow fiber membrane modules as gas–liquid contactors. Part 2. Mass transfer with chemical reaction, J. Membr. Sci. 78 (1993) 217–238.
[10] H.A. Rangwala, Absorption of carbon dioxide into aqueous solutions using hollow fiber membrane contactors, J. Membr. Sci. 112 (1996) 229–240.
[11] D. Bhaumik, S. Majumdar, K.K. Sirkar, Absorption of CO_2 in a transverse flow hollow fiber membrane module having a few wraps of the fiber mat, J. Membr. Sci. 138 (1998) 77–82.
[12] Y.S. Kim, S.M. Yang, Absorption of carbon dioxide through hollow fiber membranes using various aqueous absorbents, Sep. Purif. Technol. 21 (2000) 101–109.
[13] P.H.M. Feron, A.E. Jansen, CO_2 separation with polyolefin membrane contactors and dedicated absorption liquids: performances and prospects, Sep. Purif. Technol. 27 (2002) 231–242.
[14] P.S. Kumar, J.A. Hogendoorn, P.H.M. Feron, G.F. Versteeg, New absorption liquids for the removal of CO_2 from dilute gas streams using membrane contactors, Chem. Eng. Sci. 57 (2002) 1639–1651.
[15] V.Y. Dindore, D.W.F. Brilman, P.H.M. Feron, G.F. Versteeg, CO_2 absorption at elevated pressures using a hollow fiber membrane contactor, J. Membr. Sci. 235 (2004) 99–109.
[16] R. Wang, H.Y. Zhang, P.H.M. Feron, D.T. Liang, Influence of membrane wetting on the CO_2 capture in microporous hollow fiber membrane contactors, Sep. Purif. Technol. 46 (2005) 33–40.

[17] V.Y. Dindore, D.W.F. Brilman, G.F. Versteeg, Modeling of cross-flow membrane contactors: physical mass transfer processes, J. Membr. Sci. 251 (2005) 209–222.
[18] Y. Lee, R.D. Noble, B.Y. Yeom, Y.I. Park, K.H. Lee, Analysis of CO_2 removal by hollow fiber membrane contactors, J. Membr. Sci. 194 (2001) 57–67.
[19] P.S. Kumar, J.A. Hogendoorn, P.H.M. Feron, G.F. Versteeg, Approximate solution to predict the enhancement factor for the reactive absorption of a gas in a liquid flowing through a microporous membrane hollow fiber, J. Membr. Sci. 213 (2003) 231–245.
[20] S.H. Yeon, B. Sea, Y.I. Park, K.H. Lee, Determination of mass transfer in PVDF hollow fiber membranes for CO_2 absorption, Sep. Sci. Technol. 38 (2003) 271–293.
[21] R. Wang, D.F. Li, D.T. Liang, Modeling of CO_2 capture by three typical amine solutions in hollow fiber membrane contactors, Chem. Eng. Process. 43 (2004) 849–856.
[22] S. Karoor, Gas separation using microporous hollow fiber membranes, Ph.D. Dissertation, Stevens Institute of Technology, Hoboken, NJ, 1992.
[23] K.A. Hoff, O. Juliussen, O.F. Pedersen, Modeling and experimental study of carbon dioxide absorption in aqueous alkanolamine solutions using a membrane contactor, Ind. Eng. Chem. Res. 43 (2004) 4908–4921.
[24] M. Caplow, Kinetics of carbamate formation and breakdown, J. Am. Chem. Soc. 90 (1968) 6705–6803.
[25] P.V. Danckwerts, The reaction of CO_2 with ethanolamines, Chem. Eng. Sci. 34 (1979) 443–446.
[26] P.M.M. Blauwhoff, G.F. Versteeg, W.P.M. van Swaaij, A study on the reaction between CO_2 and alkanolamines in aqueous solutions, Chem. Eng. Sci. 39 (1984) 207–235.
[27] G.F. Versteeg, W.P.M. van Swaaij, On the kinectics between CO_2 and alkanolamines both in aqueous and non-aqueous solutions. I. Primary and secondary amines, Chem. Eng. Sci. 43 (1988) 573–585.
[28] G.F. Versteeg, M.H. Oyevaar, The reaction between CO_2 and diethanolamine at 298 K, Chem. Eng. Sci. 44 (1989) 1264–1268.
[29] H. Bosch, G.F. Versteeg, W.P.M. van Swaaij, Kinetics of the reaction of CO_2 with the sterically hindered amine 2-amino-2-methylpropanol at 298 K, Chem. Eng. Sci. 45 (1990) 1167–1173.
[30] R.J. Little, G.F. Versteeg, W.P.M. van Swaaij, Kinetics of CO_2 with primary and secondary amines in aqueous solutions. II. Influence of temperature on zwitterions formation and deprotonation rates, Chem. Eng. Sci. 47 (1992) 2037–2045.
[31] S. Xu, Y.W. Wang, F.D. Otto, A.E. Mather, Kinetics of the reaction of carbon dioxide with 2-amino-2-methyl-1-propanol solutions, Chem. Eng. Sci. 51 (1996) 841–850.
[32] G.F. Verteeg, W.P.M. van Swaaij, Solubility and diffusivity of acid gases (CO_2, N_2O) in aqueous alkanolamine solutions, J. Chem. Eng. Data 33 (1988) 29–34.
[33] J. Happel, Viscous flow relative to arrays of cylinders, AIChE J. 5 (1959) 174–177.
[34] E.L. Cussler, Values of diffusion coefficients, in: Diffusion Mass Transfer in Fluid Systems, 2nd ed., Cambridge University Press, Cambridge, UK, 1997 (Chapter 5).
[35] K.E. Brenan, S.L. Campbell, L.R. Petzold, Numerical Solution of Initial-value Problems in Differential–Algebraic Equations, North-Holland, New York, 1989.